



Staggered Field in Quantum Antiferromagnetic $S = 1/2$ Spin Chain Probed by High-Frequency EPR (the Case of Doped CuGeO_3)

S. V. Demishev^{1,2} · A. V. Semeno¹ · H. Ohta³

Received: 20 August 2020 / Revised: 6 October 2020 / Accepted: 11 October 2020 /

Published online: 23 October 2020

© Springer-Verlag GmbH Austria, part of Springer Nature 2020

Abstract

The flashback of the investigation of CuGeO_3 doped with magnetic impurities carried out by high-frequency EPR brings to light physics still actual for one-dimensional $S = 1/2$ quantum spin chains and covering a vast area from disorder-driven quantum critical phenomena to a new type of magnetic oscillations. It is shown that a key opening the door for a better understanding of this field of research is the Oshikawa and Affleck (OA) theory and, especially, following from it the universal link between the line width and g factor. The most puzzling problem appears around the staggered field, which contributes to different physical properties and serves as a driving force in the onset of anomalous growth of the line width and g factor at low temperatures. Accent is made on unsolved problems still providing a challenge for the theoretical explanation, including the genesis of the staggered field in doped systems, the contribution of the staggered magnetization to the integrated intensity, and spin susceptibility of a Griffiths phase and its magnetic properties on the nanoscale. A new type of magnetic oscillations, having explanation neither in OA theory nor within the framework of the semi-classical magnetization motion, is described in detail. This experimental finding poses the most difficult case and a touchstone for theory, as long as the corresponding modes of magnetic oscillations may be likely treated as violating Landau–Lifshits equation of motion.

✉ S. V. Demishev
demis@lt.gpi.ru

¹ Prokhorov General Physics Institute of the Russian Academy of Sciences, Vavilov Street, 38, Moscow 119991, Russia

² National Research University Higher School of Economics, Myasnitskaya, 20, Moscow 101000, Russia

³ Molecular Photoscience Research Center, Kobe University, 1-1 Rokkodai, Nada, Kobe 657-8501, Japan

1 Introduction

In the present review, we are aimed at revisiting germanium cuprate, CuGeO_3 , a remarkable spin chain system. As long as the discovery of spin-Peierls (SP) transition at $T_{\text{SP}} \sim 14$ K in this material occurred a quarter-century ago [1, 2] and the corresponding boom in research is completely over at a moment, there should be strong motivation for taking such historical excursion to the time “when Queen Anne was alive”. In general, the reasons are (1) unsolved problems and unexplained effects, (2) impact on physics of antiferromagnetic (AF) $S=1/2$ one-dimensional (1D) spin chains, and (3) issues important for studies of quantum spin chains by electron paramagnetic resonance (EPR). Thus, we hope that this program will help in modern research avoiding the trap like Queen Anne is dead.

First of all, CuGeO_3 is the first and perhaps still the best example of inorganic spin-Peierls material. As long as spin-Peierls phenomenon is a fingerprint of 1D AF $S=1/2$ spin chain, this means that this three-dimensional solid is a 1D real guest in our 3D world. This happens in spite of the presence of noticeable interactions between chains which are related as $J_c:J_b:J_a \sim 1:0.1:0.01$ [3] (where J_c , J_b , and J_a denote in-chain, inter-chain in-plane, and inter-plane exchange integrals, Fig. 1). It is important that CuGeO_3 as an inorganic material opens an opportunity to study doped material, i.e., investigate the influence of disorder on spin chain properties [4, 5]. The doping problem was attempted to understand in the framework of universal scenario [6], according to which disorder suppresses the spin-Peierls transition and leads first to co-existence of SP state with AF order and then to the onset of the Neel state. Interestingly, it believes that this scenario did not depend on the impurity type.

This theoretically supported opportunity may be true for Zn and Si dopants [4–6] but the situation becomes entirely different for the case of iron, cobalt, and manganese magnetic impurities, which substitute copper in spin chains. These impurities suppress any type of long-range magnetic order, but keep 1D character of the spin system dynamic magnetic response and result in the onset of a disorder-driven quantum critical regime. Considered type of doping allows scrutinizing Oshikawa and Affleck (OA) theory for EPR in 1D $S=1/2$ AF spin chains, which is an exact solution in contrast with still widely used old exchange narrowing theory. A consequence

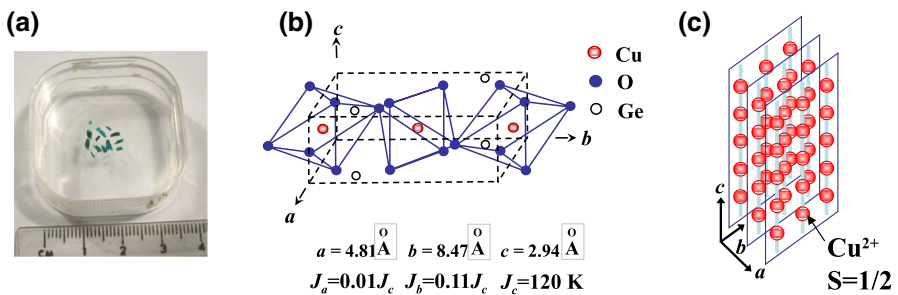


Fig. 1 Single crystals of CuGeO_3 doped with magnetic impurities prepared by the self-flux technique (a); crystal structure of CuGeO_3 (b); quantum spin chains in CuGeO_3 consisting of $S=1/2$ Cu^{2+} magnetic ions (c)

of OA theory is the appearance of new universal relations linking the g factor and line width. On the other hand, just OA theory provides an additional window to look at magnetic interactions in a disordered system. Moreover, in this family of dopants, it is possible to find systems with unusual magnetic resonance, looking like a violation of the famous Landau–Lifshits equation of motion. All this reach and up to now not fully understood physics can be labeled as a staggered field problem.

2 Doping of CuGeO_3 with Fe, Co, Mn, and Disorder-Induced Quantum Critical Behavior

The effect of doping of Cu^{2+} chains ($S=1/2$) with Fe^{2+} ($S=2$), Co^{2+} ($S=3/2$) and Mn^{2+} ($S=5/2$) in CuGeO_3 single crystals synthesized by self-flux technique was examined by EPR wide frequency range 0.06–0.4 THz in magnetic field up to 16 T. The lowest temperature achieved in some experiments was ~ 0.35 K. Both cavity and quasi-optical techniques were used; in some cases, the study of dynamic magnetic properties was accompanied by static magnetic susceptibility measurements with the help of SQUID magnetometer.

Examples of the EPR spectra are presented in Fig. 2 (samples doped with 1% of Fe), Fig. 3 (samples doped with 2% of Co), and Fig. 4 (samples doped with 0.9% of Mn). All spectra are presented by a single Lorentzian line corresponding to doped Cu^{2+} chain, except the case of cobalt impurity (Fig. 3), where apart from resonance B due to Cu^{2+} chain, there is resonance B representing new collective excitation to be discussed in the last section of this paper. In all cases, the dispersion of the modes is linear by a magnetic field (see example in Fig. 3). In this section, we will first consider temperature dependence of the integrated intensity $I(T)$, which is proportional to spin susceptibility $\chi(T)$ of Cu^{2+} chains.

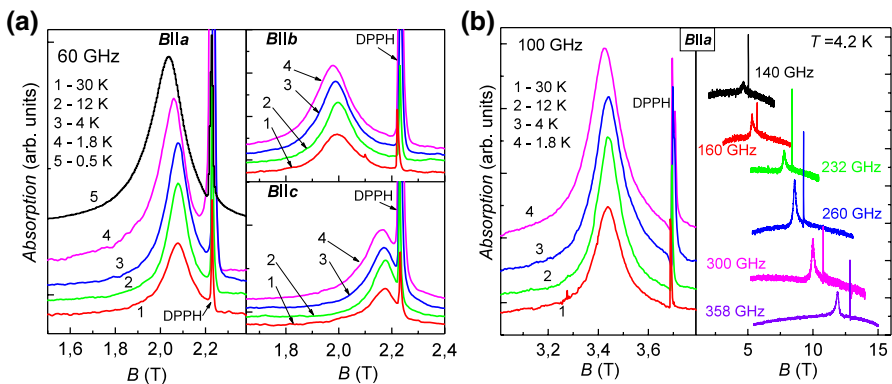


Fig. 2 EPR spectra for $\text{CuGeO}_3\text{:Fe}$ sample in 60 GHz cavity experiments for different alignment of the magnetic field with respect to crystal axes (a) and EPR spectra for Fe-doped sample at higher frequencies (b). Left part of the (b) corresponds to 100 GHz cavity experiments; right part of the (b) displays the quasi-optical EPR spectra

Fig. 3 Resonant magnetoabsorption spectrum for Co-doped CuGeO_3 (a) and field dependence of the resonant frequencies for modes A and B (b) (from Ref. [10])

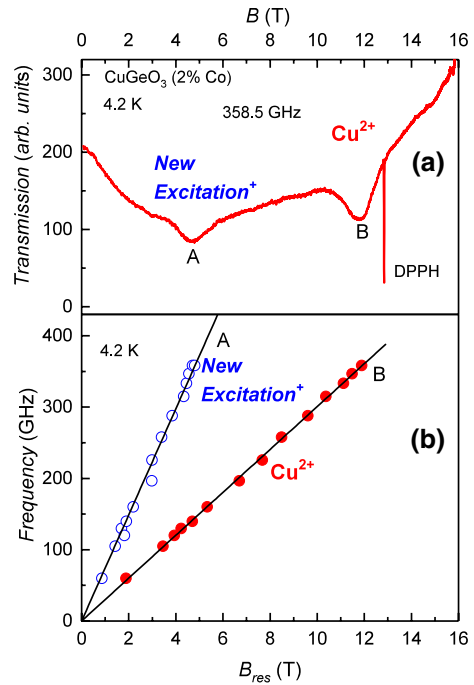
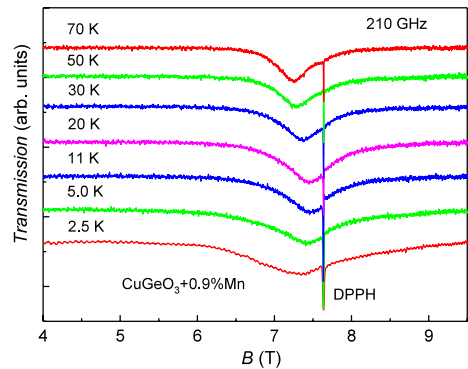


Fig. 4 EPR spectra in Mn-doped CuGeO_3 (from Ref. [11])



It has been shown [7–10] that doping of the spin-Peierls compound CuGeO_3 with magnetic impurities such as iron and cobalt gives rise to disorder driven quantum critical (QC) phenomena. The insertion of these magnetic ions at a concentration level $x=1-2\%$ into antiferromagnetic (AF) Cu^{2+} quantum spin chains ($S=1/2$) has led to a reduction of both the spin-Peierls and Neel transitions at least down to 1.8 K or 0.5 K in the cases of Co and Fe respectively [7–10]. Ground states for $\text{CuGeO}_3:\text{Fe}$ and $\text{CuGeO}_3:\text{Co}$ are found to be a disorder-induced quantum critical Griffiths phase (GP) [12]. The fingerprint of this type of quantum criticality is a power law for low-temperature asymptotic of the magnetic susceptibility [13–16]:

$$\chi(T) \sim 1/T^\alpha, \tag{1}$$

different from the Curie–Weiss or Bonner–Fisher laws. In Eq. (1), the exponent satisfies the condition $\alpha < 1$ and is non-universal depending on the random field characteristics [13].

Power divergence of the magnetic susceptibility Eq. (1) is a consequence of the power distribution function of exchange energy and reflects low-temperature correlations in spin system. The explicit evaluation of the $\chi(T)$ for QC system is hardly possible at an arbitrary temperature and thus only behavior in the limit $T \rightarrow 0$ corresponding to Eq. (1) is obtained in the majority of works [13–16].

However, as it was pointed out by Bray [13], the distribution function of J exists at all temperatures and thus may affect both low temperature (correlated quantum critical spin clusters) and high temperature (quasi-free spins) magnetic properties. In this sense, the high-temperature region should also contain information about QC regime. An approach, which allows the description of the magnetic susceptibility of a disorder-driven QC system with AF interactions at an arbitrary temperature, has been recently suggested in [17–19]. In this model, a disordered magnetic system is considered as a set of identical volume elements, each characterized by the Néel temperature $T_N \sim J$ and the paramagnetic temperature $\theta = -T_N/\epsilon$. For three-dimensional antiferromagnet, the parameter ϵ may be expressed through the molecular field constants [20], but in the model [17–19] it has a more general sense of being a degree of suppression of ordering temperature and hence can be treated as a possible disorder measure.

The magnetic susceptibility of each volume element at $T > T_N$ is described by the Curie–Weiss law [17–19]:

$$\chi = C/(T + T_N/\epsilon), \tag{2}$$

and at $T < T_N$ decreases according to the law:

$$\chi = C(T/T_N)^\gamma/[T_N(1 + 1/\epsilon)]. \tag{3}$$

Apart from the standard values $\gamma = 0$ and 1 [20], the case $\gamma \gg 1$, which simulates the opening of the spin gap can be considered [17, 19]. In the described model the Curie constant C and parameter ϵ are taken identical for all volume elements, and the Néel temperature T_N of a volume element is a random quantity limited from above $T_N < T_m$ with the distribution function [17–19]:

$$w(T_N) = (1 - \xi)(T_m/T_N)^\xi/T_m. \tag{4}$$

Then the magnetic susceptibility of the system is given by [17–19]:

$$\chi(T) = \frac{C}{T} D_\xi(T\epsilon/T_m) \approx \frac{C}{T + \theta_*} \quad (T > T_m), \tag{5}$$

$$\chi(T) = \frac{C}{T_m} D_\xi(\epsilon) \left(\frac{T_m}{T}\right)^\xi F(\epsilon, \xi, \gamma, T/T_m) \quad (T < T_m), \tag{6}$$

where

$$D_{\xi}(y) = 1 - (1 - \xi) \int_0^1 \frac{t^{1-\xi}}{t+y} dt, \quad (7)$$

and

$$F_{\xi}(\varepsilon, \xi, \gamma, y) = 1 + \frac{1 - \xi}{(1 + a)D_{\xi}(1/a)(\gamma + \xi)} (1 - y^{\gamma+\xi}). \quad (8)$$

For $T > T_m$ the temperature dependence of $\chi(T)$ is close to Curie–Weiss law with effective paramagnetic temperature depending on the considered temperature interval. In the vicinity of T_m

$$\theta * /T_m = [\varepsilon(1 - \xi)f(\varepsilon, \xi)]^{-1} - 1, \quad (9)$$

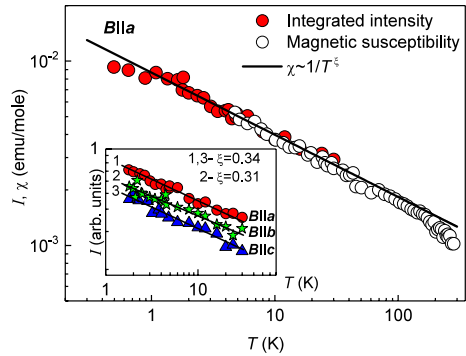
where

$$f(\varepsilon, \xi) = -\frac{1}{\xi} - \sum_{r=1}^{\infty} (-1)^r \frac{\varepsilon^r}{r + \xi} + \frac{\pi}{\varepsilon^{\xi} \sin[\pi(1 - \xi)]}. \quad (10)$$

For $T < T_m$ the Eq. (1) is valid in the limit $T \rightarrow 0$ as expected from the exact models [13–16]. In the considered approach, a decrease in temperature in the range $T < T_m$ results in “scanning” over the random T_N of volume elements. If $T < T_N$, the magnetic contribution of the corresponding volume elements freezes out due to the transition to the magnetically ordered state and the pseudo-Curie–Weiss behavior gives way to the power dependence of the magnetic susceptibility for the whole sample. Therefore, the spin clusters with a higher (as compared to the average value) degree of correlation, which determines according to [12–16] that the Griffiths phase magnetic properties should be considered as sets of volume elements for which $T_N > T$. Apparently, a local magnetic ordering in the elementary volumes in the considered model does not suggest the onset of any long-range magnetic order in the real experimental system [17–19].

The example of experimental $I(T) \sim \chi(T)$ dependence for $\text{CuGeO}_3\text{:Fe}$ is presented in Fig. 5. It demonstrates perfect correlation between integrated intensity and static susceptibility data as well as pronounced power dependence of the magnetic susceptibility. The plot in double logarithmic coordinates allows estimating the ξ value from the slope of the linear section of $\log I = f(\log T)$ curve and thus somehow depends on the chosen temperature interval. For $\text{CuGeO}_3\text{:M}$ ($M = \text{Fe, Co}$), the estimate gives with $\xi \sim 0.3\text{--}0.34$ and $\xi \sim 0.8\text{--}0.9$ (Co) in the diapason $T < 40$ K [7–10] and lasted down to the lowest temperature. Thus, the experimental data show that disorder-driven quantum critical regime in CuGeO_3 doped with magnetic impurities is observed at temperatures, which considerably exceed all characteristic temperatures on the concentration-temperature phase diagram expected in the standard scenario of doping [6].

Fig. 5 Integrated intensity and static magnetic susceptibility in $\text{CuGeO}_3\text{:Fe}$ for *B*11a (main panel) and the effects of anisotropy on the exponent describing temperature dependence of magnetic susceptibility in the Griffiths phase (inset). From Ref. [9]



EPR measurements may provide information about anisotropy of $I(T) \sim \chi(T)$. Inset in Fig. 5 shows that the exponent ξ is the same for magnetic field alignment **B**11a and **B**11c, whereas this parameter is reduced by $\sim 10\%$ for **B**11b.

The value of exponent ξ may be refined by application of the model described above. It follows from Fig. 6 that Eqs. (5)–(8) allow reproduction of the experimental dependence in the whole studied range, where temperature varies up to two orders of magnitude, giving $\xi \approx 0.3$ (Fe) and $\xi \approx 0.8$ (Co). In the latter case, the exponent is too close to unity to distinguish between different possible γ values. At the same time, in Fe-doped sample, the better description of the experiment may be achieved for $\gamma \sim 10$ corresponding to the opening of a spin gap in clusters. It is interesting that for $\text{CuGeO}_3\text{:Fe}$ and $\text{CuGeO}_3\text{:Co}$, the characteristic temperature T_m equals 120 K and coincides with the magnitude of exchange integral J_c in chains [3]. Thus, the disorder induced by doping leads to a reduction of exchange integrals in chains and causes separation of magnetic systems into spin clusters. It is interesting that considered ansatz allows estimating the size of spin clusters $\sim 10\text{--}100$ nm [17] and thus QC Griffiths phase in CuGeO_3 is “constructed” from magnetic nanoclusters.

The case of Mn-doped CuGeO_3 is more complicated [11]. As follows from Fig. 7, the asymptotic power law Eq. (1) with $\xi \sim 0.7\text{--}0.8$, which is a fingerprint for

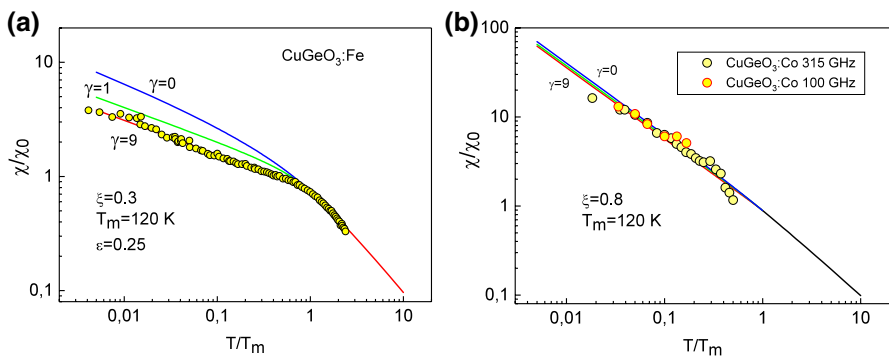


Fig. 6 Analysis of temperature dependence of integrated intensity and static magnetic susceptibility in spin cluster model of Griffiths phase [17–19], for $\text{CuGeO}_3\text{:Fe}$ (a) and $\text{CuGeO}_3\text{:Co}$ (b). See text for details

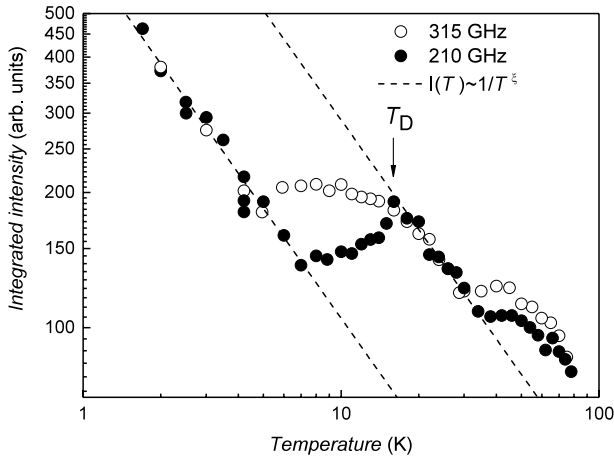


Fig. 7 Temperature dependence of integrated intensity for $\text{CuGeO}_3\text{:Mn}$ at various frequencies (from Ref. [11])

the disorder-driven QC regime, begins below ~ 40 K. In the vicinity of the characteristic temperature $T_D = 16$ K, the integrated intensity starts to deviate from the power law (Fig. 7). The value of T_D is close to the spin-Peierls transition temperature $T_{SP} \sim 14$ K in pure CuGeO_3 but somewhat higher.

It is interesting that below $T \sim 7$ K for the frequency 210 GHz and below $T \sim 5$ K for the frequency 315 GHz, a power law with the same ξ is restored and holds up to the lowest temperature studied (Fig. 7). The observed re-entrant $I(T)$ dependence is different from that for $\text{CuGeO}_3\text{:Fe}$ and $\text{CuGeO}_3\text{:Co}$ (Figs. 5, 6) and thus reflects a characteristic effect of the Mn impurity.

Such an unusual behavior may be qualitatively explained as follows. As long as at T_D the integrated intensity [and hence $\chi(T)$] starts to decrease this characteristic temperature may be attributed to dimerisation of the quantum spin chains. Apparently, the possible spin-Peierls transition in $\text{CuGeO}_3\text{:Mn}$ occurs within the Griffiths phase in the developed QC regime, i.e., when the magnetic subsystem is divided into spin clusters with the different coupling constants. As long as the temperature lowering leads to an increase of the cluster size [13–57], a transition into the dimerised state may be allowed for the chains belonging to clusters with sizes exceeding the coherence length. Below T_D , the magnetic contribution from dimerised Cu^{2+} chains vanishes rapidly due to the opening of a spin gap, and only the chains in the QC state contribute to the susceptibility. Therefore, a power law for $\chi(T)$ and $I(T)$ may be restored at $T < T_D$. As long as in the disorder-driven QC regime, the index ξ depends on the space dimension and dynamic exponent connecting time and length scales [21]; it is possible to expect a re-entrant quantum criticality at $T < T_D$ with the same value of the critical exponent as observed experimentally (Fig. 7). Moreover, the fact, that in our case the condition $T_D > T_{SP}$ is fulfilled, may be a consequence of the change of the phonon–magnon interaction in finite spin clusters.

The fitting of $I(T)$ for the region $T > T_D$ with the help of the model Eqs. (5)–(8) provides $\xi = 0.7$ and is consistent with $T_m = 120$ K supporting the

general character of the considered approach for the description of magnetic susceptibility of a Griffiths phase.

To conclude this section, it is possible to notice that different impurities in CuGeO_3 behave in a different way, which is far from the universal scenario of doping [6], but is pretty close to that one may generally expect in condensed matter physics. At this point, we may be also asked about the above-promised staggered field that is not mentioned in this section. Actually, it is already here but in a hidden manner, which will be clear from further consideration.

3 Oshikawa and Affleck Theory and the Advent of the Staggered Field

3.1 Universal Relation

The classical theory of the EPR of isolated ions suggests that the line width w decreases when the temperature is lowered because of the diminishing of the thermal broadening of the energy levels [22]. The first, theoretical approaches developed for one-dimensional (1D) interacting spin systems [23–25], although predicting more complicated behavior of w , could not explain some of the experimental observations in one-dimensional systems, like *increase* of $w(T)$ in Cu-benzoate in the limit $T \rightarrow 0$ [26]. We have to notice that this behavior is from time to time observed in various low-dimensional spin systems, but often is left without interpretation.

This type of anomaly had no explanation for almost 30 years until Oshikawa and Affleck have proposed a new theory of EPR for 1D $S=1/2$ antiferromagnetic chains [27, 28]. They have suggested that there are only two important contributions to the unperturbed spin Hamiltonian, namely the exchange anisotropy and the staggered field which break the initial symmetry and, therefore, give rise to a finite EPR line width [27, 28]. In both cases, the Lorentzian line shape is expected. For the exchange anisotropy contribution at low temperatures, OA theory gives [28]:

$$w(T) = w_{\text{ea}} = \frac{b\delta^2 k_{\text{B}} T}{J^2 \mu_{\text{B}}}, \quad (11)$$

where J is the exchange integral and δ denotes the exchange anisotropy constant. In the opposite limit of high temperatures, $k_{\text{B}} T \gg J$, the line width saturates [28]:

$$w_{\text{ea}} \approx \frac{a\delta^2}{J\mu_{\text{B}}}. \quad (11a)$$

In Eqs. (11) and (11a), numerical coefficients a and b are of the order of unity [28]. It is clear that the contribution from the exchange anisotropy corresponds to the general expectation [22], i.e., $w(T \rightarrow 0) \rightarrow 0$.

The departure from the classical case appears when the staggered field is taken into account [27, 28]:

$$w(T) = w_{\text{sf}} = 0.68571 \frac{J\mu_B h^2}{(k_B T)^2} \ln \left(\frac{J}{k_B T} \right), \quad (12)$$

and $w(T)$ diverges as $1/T^2$ at $T \rightarrow 0$. In the latter equation, h gives the magnitude of the staggered field. The divergence of w_{sf} is accompanied by the corresponding shift of the resonant frequency $\delta\omega \sim h^2 B/T^3$ [27, 28].

Demishev et al. [29] pointed out that in OA calculation, external magnetic field $B = \text{const}$ and the resonant frequency is given by $\omega = g\mu_B B/\hbar$. Thus, the frequency shift $\delta\omega$ can be expressed in terms of the correction Δg to effective g factor:

$$\Delta g = \Delta g_{\text{sf}} = 0.344057 \frac{J\mu_B^2 h^2}{(k_B T)^3} \ln \left(\frac{J}{k_B T} \right). \quad (13)$$

Therefore, in the case of the staggered field, the OA theory predicts both the anomalous temperature dependence of the line width and the low-temperature increase of g factor. As the line width, the low-temperature increase of the g factor is also observed from time to time in EPR studies of various low-dimensional spin systems.

Combination of Eqs. (12) and (13) leads to the *universal* relation [29], which was missed in the initial OA theory:

$$\frac{w_{\text{sf}}}{\Delta g_{\text{sf}}} = 1.99 \frac{k_B T}{\mu_B}. \quad (14)$$

Equation (14) links $w_{\text{sf}}(T)$ and $\Delta g_{\text{sf}}(T)$ and does not depend on the staggered field magnitude and the exchange integral and therefore of the solid type. As long as Eq. (14) appears to be unrestrained by the experimental object, this consequence of the OA theory, first of all, seems to be a very useful experimental probe of staggered fields in one-dimensional magnets. Second, the universal link between line width and g factor is unique among EPR theories and hence constitutes a strong statement, which experimental check can be considered as verification of correctness of the approach [27, 28] used by Oshikawa and Affleck.

In the initial studies [27, 28], Eq. (11) was compared with the experiments for CuGeO_3 and $\alpha\text{-NaV}_2\text{O}_5$. However, the regime of the line width saturation (Eq. 11a) has not been analyzed in [27, 28]. Moreover, the use of the experimental data for $\alpha\text{-NaV}_2\text{O}_5$ is controversial, as long as this material possesses a ladder magnetic structure and, hence, is not really one-dimensional [30]. Equation (12) has been used in [27, 28] to fit the data for Cu-benzoate from Ref. [26]. It was found that OA theory provides qualitative agreement with the experiment [27, 28]. Nevertheless, at low temperatures, a considerable discrepancy between Eq. (12) and the experimental dependence $w(T)$ could be noted. A more recent experimental study of Cu-benzoate [31] was mainly focused on the investigation of the breathing mode in this material although a qualitative agreement with the OA theory predictions for the case of the staggered field was reported [31].

The universal consequence of OA theory was first examined in [29]. The data displayed in Fig. 8 show that doping with magnetic impurities Fe and Co induces sections of low-temperature growth of the line width (main panel) and g factor (inset). At the same time, high-temperature part of $w(T)$ follows the behavior expected for exchange anisotropy contribution (Eqs. 11, 11a). This type of dependence is qualitatively the same as in the pure (undoped) crystal, and CuGeO₃ sample doped with Ti non-magnetic impurity, where spin-Peierls transition is conserved at $T_{SP} \sim 14$ K. The following simple interpolating expression to fit the high-temperature part of $w(T)$ was suggested in [29]:

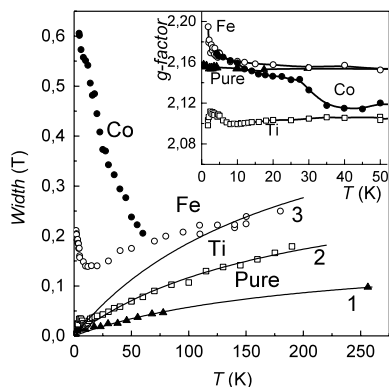
$$w_{ea} = \frac{a\delta^2 k_B T}{J_c \mu_B \left(k_B T + \frac{aJ_c}{b} \right)}, \tag{15}$$

with $J_c = 120$ K. Equation (15) corresponds to the theoretical results Eqs. (11) and (11a) for $J_c \gg k_B T$ and $J_c \ll k_B T$, respectively, and the ratio a/b sets the region of the crossover from the low-temperature to high-temperature asymptotic. It was shown that Eq. (15) fits the experimental data well at $T > T_{SP}$ for pure and Ti-doped samples (curves 1 and 2 respectively in Fig. 8). Interestingly, in both cases, the same ratio value $a/b \approx 1.65 \pm 0.15$ has been obtained. Consequently, the increase of the line width in the doped sample is caused by the growth of the exchange anisotropy constant δ . Assuming $a \sim 1$, one gets an estimate $\delta/J_c \sim 0.03$ for the pure sample (curve 1 in Fig. 8) and $\delta/J_c \sim 0.05$ for the Ti-doped sample (curve 2 in Fig. 8).

Equation (15) was used in [29] to fit the high-temperature part of $w(T)$ for the Fe-doped sample. In the framework of this procedure, the further increase of δ reaching the value of $\delta/J \sim 0.06$ may be expected [29] (see curve 3 in Fig. 8). However, the application of Eq. (15) is controversial, as long as in CuGeO₃:Fe, there is a distribution of exchange energy due to the presence of a Griffiths phase (see the previous section). Nevertheless, it seems that Eq. (15) at least with some effective parameters may be used for approximation of the experimental data even in the disordered case.

The next idea of [29] was to subtract $w_{ea}(T)$ from $w(T)$ and obtain low-temperature divergent $w_{sf}(T)$ and compare it with the universal relation Eq. (14). The ratio $w(T)/\Delta g(T)$ for CuGeO₃ was calculated from the data in Fig. 8 assuming $\Delta g(T) = g$

Fig. 8 Line width and g factor in pure, Ti-doped, Fe-doped and Co-doped CuGeO₃ (from Ref. [29])



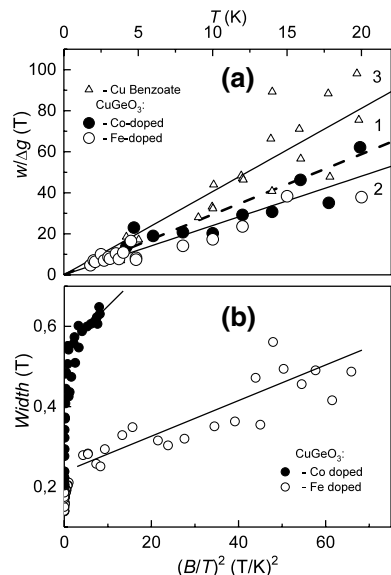
($T - g(30\text{ K})$) [29]. The obtained values of $w(T)/\Delta g(T)$ are plotted as a function of temperature in Fig. 9a. In spite of the big difference in the parameters of EPR lines for Co and Fe impurities (Fig. 8), the ratio $w(T)/\Delta g(T)$ behaves very similar both for Co and Fe doped samples, and it can be described by the same linear temperature dependence at $T < 20\text{ K}$. Apparently, for the Co-doped case, the ERP data for the resonance on Cu^{2+} chains were used.

It was found in [29] that the best fit for experimental data for CuGeO_3 is provided by $w(T)/\Delta g(T) = (1.63 \pm 0.07) k_B T / \mu_B$ (curve 2 in Fig. 9a) with the numerical coefficient different from the theoretical one (curve 1 in Fig. 9a) by 20%. The data for Cu-benzoate from [31] plotted in the same coordinates also follow linear dependence corresponding to the approximation $w(T)/\Delta g(T) = (2.75 \pm 0.15) k_B T / \mu_B$ (curve 3 in Fig. 9a) with the slope remarkably (1.7 times) different from CuGeO_3 case. Note that OA theory underestimates the coefficient observed for Cu-benzoate by 40%.

We see that CuGeO_3 doped with magnetic impurities provides better coincidence with the universal consequence of OA theory than Cu-benzoate, although the latter compound is believed to be a perfect experimental realization of 1D Heisenberg chain with a staggered field [32, 33]. This is amazing as long as OA theory does not account for the dispersion of the exchange energy in $\text{CuGeO}_3:\text{Fe}$ and $\text{CuGeO}_3:\text{Co}$. The result of analysis in [29] means that the universal relation Eq. (14) is not only independent of J in chains but is not much sensitive to J distribution function. Therefore, Eq. (14) may have more general meaning coming out from the limits of OA theory.

An additional argument favoring the applicability of the OA theory to the case of CuGeO_3 doped with magnetic impurities arises from the magnetic field dependence of EPR line parameters. Assuming expected proportionality to the external field, $h \sim B$ [27, 28], Eq. (12) suggests a low-temperature asymptotic $w \sim (B_{\text{res}}/T)^2$,

Fig. 9 Universal relation between line width and g factor (a) and quadratic asymptotic for the line width following from OA theory (b) (from Ref. [29]). See text for details



where B_{res} is a magnetic resonance field at a given frequency. The corresponding analysis in [29] provides the evidence that square low-temperature/high-field asymptotic really exists in CuGeO_3 doped with magnetic impurities (Fig. 9b) and thus OA theory can be applied in the considered case for the description of the anomalous low-temperature behavior of the line width caused by the staggered field.

The OA theory considered above is useful for the explanation of EPR data in $\text{CuGeO}_3:\text{Fe}$ and $\text{CuGeO}_3:\text{Co}$, but the situation becomes more complicated for $\text{CuGeO}_3:\text{Mn}$ [11]. In the latter material, the simultaneous low-temperature growth of the line width and g factor is observed as well. However, the explanation of the temperature dependency of these parameters is possible, assuming the crossover from the high-temperature semi-classical Nagata and Tazuke [34, 35] limit to the low-temperature quantum case described by Oshikawa and Affleck theory. In this way, the simultaneous description of the line width and g factor was achieved in [11] for the frequencies range ~ 200 GHz. Deviations from this model observed in Mn-doped system at higher frequencies [11] may be explained by an enhancement of antiferromagnetic interactions in high magnetic fields. This effect will be considered in detail in the next section.

As a final remark, it should be mentioned that OA theory describes 1D spin chain. The applicability of this model indicates that magnetic system of CuGeO_3 doped with magnetic impurities keeps predominantly one-dimensional character at least in a dynamical sense. We see that even in the case of suppressed spin-Peierls transition, there is another marker of one-dimensionality and this marker is a universal relation linking line width and g factor due to the presence of the staggered field.

3.2 The Competition Between Staggered Field and Antiferromagnetic Interaction

The method of the analysis of EPR data presented in Sect. 3.1 may be improved [36, 37]. Indeed, in the presence of the exchange anisotropy and staggered field, the line width and g factor at low temperatures in the OA theory are given by

$$w(T) = w_{\text{ea}}(T) + w_{\text{sf}}(T) = A \cdot T + C \cdot h^2 \cdot T^{-2}, \quad (16a)$$

$$g(T) = g_0 + g_{\text{sf}}(T) = g_0 + D \cdot h^2 \cdot T^{-3}, \quad (16b)$$

where h denotes the magnitude of the staggered field, and A , C and D stand for the quantity having weak temperature dependence and defined by the Eqs. (11)–(13). Low-temperature growth of $w(T)$ and $g(T)$ is caused by staggered field and these parameters are strongly correlated, i.e., the values C and D are different by numerical coefficient [29]. Thus, instead of the direct use of the universal relation Eq. (14), it is possible to consider the Owikawa–Affleck function [36, 37]

$$f_{\text{OA}}(T) = w(T)/[\Delta g(T) \cdot T] \equiv A * \cdot (T^3/h^2) + C_{\text{OA}}, \quad (17)$$

where $\Delta g(T) = g(T) - g_0$, $A^* = A/D$ and C_{OA} is the universal constant in the OA theory, which does not depend on the exchange integral and staggered field magnitude: $C_{\text{OA}} = 1.99 \cdot k_B/\mu_B$ (see Eq. 14).

Equation (17) suggests that in 1D case $f_{OA} \rightarrow C_{OA}$ when $T \rightarrow 0$. This behavior changes dramatically when a possibility of 3D AF ordering is taken into account [10], as long as approaching the Neel point T_N from above leads to the line width divergence $W \sim (T - T_N)^{-3/4}$ [24, 25]. A possible correction to the g factor may be attributed to the difference between local and external magnetic field, i.e., $\Delta g(T) \sim \chi(T)$. Thus, in 3D AF model, the OA function acquires the form [36, 37]

$$f_{OA}(T) \sim [T \cdot \chi(T) \cdot (T - T_N)^{4/3}]^{-1}, \tag{18}$$

and $f_{OA}(T \rightarrow T_N) \rightarrow \infty$. Consequently, the analysis of the experimental data by the computation of OA function allows discriminating EPR line broadening caused by AF correlations and staggered field. This program was fulfilled for the Fe-doped CuGeO_3 [36, 37].

The ERP spectra were measured for different alignment of the magnetic field with respect to crystallographic directions. Both cavity and quasi-optical techniques were applied [36, 37]. The results are summarized in Fig. 10a, b, where main panels and insets display data for the line width and g factor, respectively. The temperature dependency of the line width demonstrates low-temperature minimum (Fig. 10a, b). This is in agreement with the OA theory predictions for the case when both

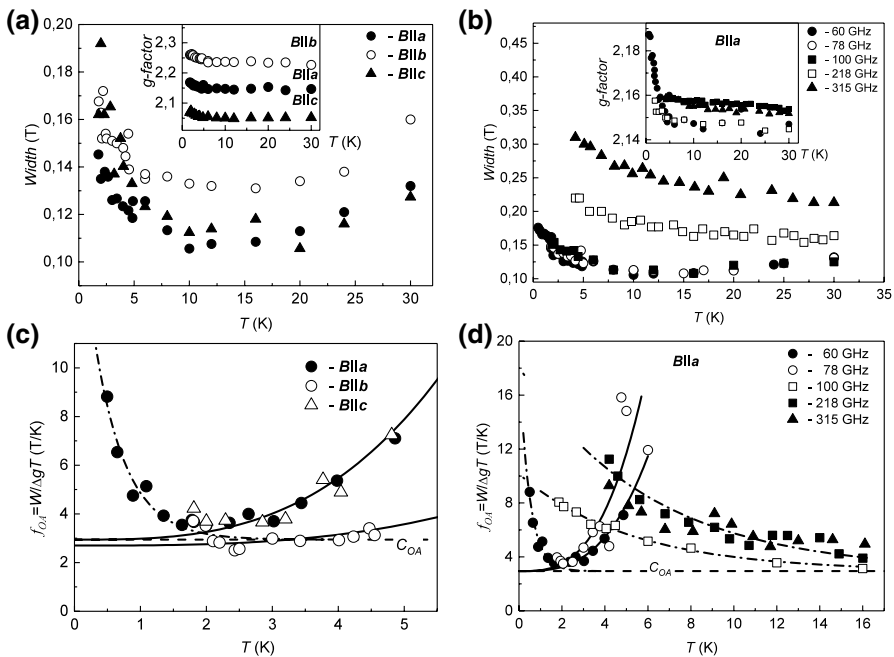


Fig. 10 Temperature dependence of line width and g factor for various orientations of the magnetic field measured at frequency 60 GHz (a) and temperature dependences of line width and g factor for $B11a$ at various frequencies (b). Panel c represents the OA function calculated from the data shown in panel (a). Points—experiment; solid lines—best fits using Eq. (17). Dashed line—universal constant in the OA theory. Dash-dot line is a fit with Eq. (18). Panel d displays the OA function calculated from the data in panel b. The signs are the same as in panel c. From Refs. [36, 37]

exchange anisotropy and staggered field effects take place (Eq. 16a). It is visible that the low-temperature increase of the g factor occurs simultaneously (Eq. 16b). The data in Fig. 10b suggest that an increase of frequency (and hence of the resonant field) induces enhancement of the line width. At the same time, for frequency range $\nu \geq 100$ GHz, the low-temperature growth of the g factor apparently slows down (inset in Fig. 10b).

To clarify mechanisms causing the broadening of the line width and temperature correction to the g factor, the OA functions were computed from the data shown in Fig. 10a, b [36, 37]. The results are presented in Fig. 10c, d respectively; solid lines are corresponding to fits using Eq. (17). In calculations, the value $\Delta g(T) = g(T) - g(30 \text{ K})$ has been used. It is visible that OA theory provides a reasonable description of the experimental data at 60 GHz for various orientations of the magnetic field in the interval $T > 2$ K. Interesting that for $B \parallel a$ and $B \parallel c$ the magnitude of the coefficient at T^3 in Eq. (17) A^*/\hbar^2 is almost equal and noticeably bigger than in case $B \parallel b$ (Fig. 10c). As long as in OA theory A^* does not depend on magnetic field orientation, this result suggests that the staggered component of the magnetic moment (and accordingly staggered field) is the biggest, when an external magnetic field is aligned along b -axis. Thus, b -axis may be treated as an “easy axis” for staggered field in CuGeO_3 structure. It is worth reminding that this direction corresponds to the strongest interchain interactions [3].

For $T < 2$ K, the experimental OA function starts to increase when the temperature is lowered and apparently deviates from the predictions of the OA theory. According to [36, 37], this behavior reflects approaching AF transition temperature in qualitative agreement with Eq. (18) (dash-dotted lines in Fig. 10c, d). Hence, the observed non-monotonous dependence of the $f_{\text{OA}}(T)$ is due to a transition from predominantly 1D behavior of Cu^{2+} chains ($T > 2$ K) to the beginning of the 3D AF correlations ($T < 2$ K).

The above consideration suggests that AF interactions in $\text{CuGeO}_3:\text{Fe}$ may become stronger for higher frequencies (magnetic fields). The data in Fig. 10d indicate that for $\nu \geq 100$ GHz at low temperature, the OA asymptotic Eq. (17) is no longer valid and the observed $f_{\text{OA}}(T)$ can be understood in the 3D AF ordering model (Eq. 18). However, the magnetic field dependence of the exchange interaction is usually small, which indicates that the observed variation of EPR parameters is quite unusual. It is possible that field-induced enhancement of AF interaction reflects properties of the Griffiths phase characterized by dispersion of exchange energies. We expect that the corrections due to the magnetic field may become comparable with the smallest AF exchange energies and thus will give way to increase of 3D AF correlations in corresponding spin clusters. As long as spin clusters with the lowest exchange energies control low-temperature behavior of doped CuGeO_3 , the strongest contribution from field-induced effects should occur at low temperatures as observed experimentally. Nevertheless, this qualitative explanation requires further theoretical clarification.

We see that OA theory provides a unique tool for studying the staggered field in AF $S=1/2$ quantum spin chain system. In $\text{CuGeO}_3:\text{Fe}$, the observed temperature dependence of the line width and g factor is formed as a result of the competition between interchain antiferromagnetic interactions in CuGeO_3 and staggered Zeeman energy, as it follows from some theoretical considerations [38]. AF interactions

become more pronounced at $T < 2$ K and in frequency range $\nu \geq 100$ GHz. We see that in the region of applicability of the OA theory, the analysis of the experimental data suggests the selected character of the \mathbf{b} -axis for the staggered field.

3.3 The Staggered Field Nature in CuGeO_3

It follows from the above consideration that there are reasons to trust in theoretical calculations [27–29] and they may be applied to the analysis of the experiment in a different way. For example, Eqs. (12) and (13) can be used for finding the staggered field magnitude. Therefore, the EPR experiments may provide direct information concerning the staggered component in the local magnetic field in the sample and its dependence on the external parameters (magnetic field, temperature, etc.).

Before starting of the suggested procedure, it is worth to think why staggered field may appear in doped CuGeO_3 . In theory staggered field is a magnetic field that changes direction alternately. In the considered works [27, 28, 38], the effects of the staggered field are described by the term in Heisenberg Hamiltonian:

$$\hat{H}_{\text{sf}} = -h \cdot \sum_{i,j,k} (-1)^i S_{i,j,k}^x \quad (19)$$

In Eq. (19) the $S_{i,j,k}^x$ is the x component of the spin 1/2 operator on numbered (i, j, k) site. As long as the external magnetic field B is aligned along the z -axis, the staggered field should lie in the direction perpendicular to the external magnetic field. In addition, it is generally assumed that staggered field magnitude is proportional to the external magnetic field $h \sim B$ [27–29, 38].

The mechanisms of the staggered field generation may be different in different experimental objects [38]. The most popular up to now is (1) the staggered component of the g tensor and (2) staggered Dzyaloshinskii–Moriya (DM) interaction [27–29, 38–41]. Both mechanisms require certain low symmetry of the crystal structure and thus can be hardly applicable to the case of the doped CuGeO_3 . Indeed, the EPR data for pure and doped with non-magnetic impurities CuGeO_3 provides no sign the staggered field anomalies in the range $T > T_{\text{SP}}$ described in the previous sections, where spin chains are homogeneous and OA theory [27, 28] is applicable. Instead, the line width in this case is terminated by exchange anisotropy [29] and $w(T) \rightarrow 0$ when $T \rightarrow 0$ [29]. Although doping of CuGeO_3 by 1% of Fe or by 2% of Co completely damps both spin-Peierls and Neel transitions, it is difficult to assume that the doping on this level can change crystal symmetry. Therefore, in our opinion, the mechanisms of the generation of the staggered field in CuGeO_3 based on staggered g tensor or DM interaction appear to be unlikely.

An alternative idea concerning the formation of the staggered field has been considered in [38]. Suppose that the low-dimensional magnetic system consists of two sublattices and possesses a strong intralattice coupling and a weak interlattice coupling. Assuming that one of the sublattices is ordered antiferromagnetically, we see that it will induce a staggered field in the other sublattice. When applying this approach to the real “1D magnets”, it is reasonable to suggest that interchain exchange may open an opportunity for the generation of the staggered field in

the sample. Coming back to the case of doped CuGeO_3 , it is necessary to remind that in this solid, the interchain interaction is not weak, being about 10% of the intrachain interaction [3]. Our hypothesis is that the doping of magnetic impurities may *locally* alter the intrachain interaction and likely affects the *local* magnetic order. As a result the spin clusters (nearly AF ordered) will be formed and these clusters will possess staggered field due to the aforementioned induction mechanism. Actually, these clusters, where the correlation of spins is stronger than average, are a characteristic feature of the Griffiths phase which develops in $\text{CuGeO}_3:\text{Fe}$ and $\text{CuGeO}_3:\text{Co}$ (Sect. 2). Thus, the local formation of the staggered field at low temperatures and quantum critical regime, for which the Griffiths phase serves as a ground state, may be closely connected.

Following the above consideration, we conclude that in CuGeO_3 , the staggered field may be spatially inhomogeneous, may depend on temperature due to magnetic impurities and interchain interactions, and, as a result, the simple linear relation between external magnetic field and staggered field, $h \sim B$, may be violated. The latter possibility is different from the case, when the staggered field is generated by staggered g tensor or DM interaction where the condition $h \sim B$ should always hold. Moreover, if the local magnetic fields in the sample originate from the magnetic moment of magnetic impurity, it is possible to expect a situation where $h(B=0) \neq 0$. The expected qualitative picture of the staggered field in CuGeO_3 doped with magnetic impurities is presented in Fig. 11.

As long as we assume that $h = h(\vec{r}, T, B)$, Eqs. (12) and (13) should be somehow averaged over spatial coordinate before applying to the considered case, taking into account both dispersion of the staggered field and exchange integrals. In addition, the temperature dependence of the staggered field may change the theoretical asymptotics $w \sim 1/T^2$ and $\Delta g \sim 1/T^3$. Nevertheless, the universal relation Eq. (14) may be less affected due to the fact that all averaged quantities are

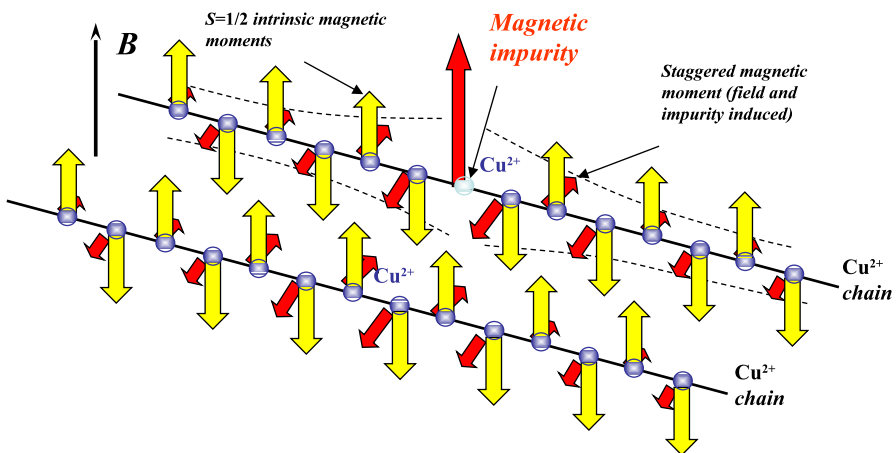


Fig. 11 Expected structure of magnetic impurity doping-induced staggered magnetization in CuGeO_3

coming into Eqs. (12) and (13) in a same way and, as a result, will still work CuGeO_3 doped with magnetic impurities (Sects. 3.1, 3.2).

Now we are ready to use Eqs. (12) and (13) as definitions of the averaged staggered field $\langle h \rangle$ and apply them to experimental data for CuGeO_3 doped with 1% of Fe or 2% of Co. The estimates following for w_{sf} and Δg defined as in [29] are presented in Fig. 12a (temperature dependence) and in Fig. 12b (field dependence). In calculations, the value $J = 120$ K [3] has been used. This choice provides a rough estimate of $\langle h \rangle$ as long as the dispersion of J in the Griffiths phase is neglected.

First of all, it is necessary to mark the good coincidence between staggered field magnitude found from the line width and g factor (Fig. 12a) which means the validity of the universal relation (14). However, the obtained quantity $\langle h \rangle$ demonstrates strong temperature dependence: the magnitude of SF decreases 7–8 times when the temperature is lowered from 20 to 4 K. At the same time, following the initial consideration [27, 28] for the cases of staggered g tensor or DM interaction, one can expect $h(T) = \text{const}$.

The field dependence of the averaged SF $\langle h \rangle$ also exhibits considerable deviations from the theoretical suppositions [27, 28]. Indeed, instead of the relation $h \sim B$ suggested in [27, 28], the experimental data in Fig. 12b are better represented by:

$$\langle h(B) \rangle = h(0) + A \cdot B, \quad (20)$$

i.e. $\langle h(B=0) \rangle \neq 0$. Therefore, in addition to the external magnetic field induced component, which is proportional to B , an intrinsic SF appears in the sample. In our opinion, this effect is specific to the case of CuGeO_3 doped with magnetic impurities as it was qualitatively described above. It is worth to note that best fits of the experimental data with Eq. (20) have provided very close values of the coefficient A , namely 0.0020 T^{-1} for Fe-doped case and 0.0024 T^{-1} for Co-doped case. Consequently, the “staggered field susceptibility”, which defines the part of the staggered field dependent on the external magnetic field, appears to be weakly dependent on the impurity studied. At the same time, data in Fig. 12b provide values $\langle h(0) \rangle \geq 0.052 \text{ T}$ and $\langle h(0) \rangle \geq 0.077 \text{ T}$ for Fe and Co impurities, respectively. This

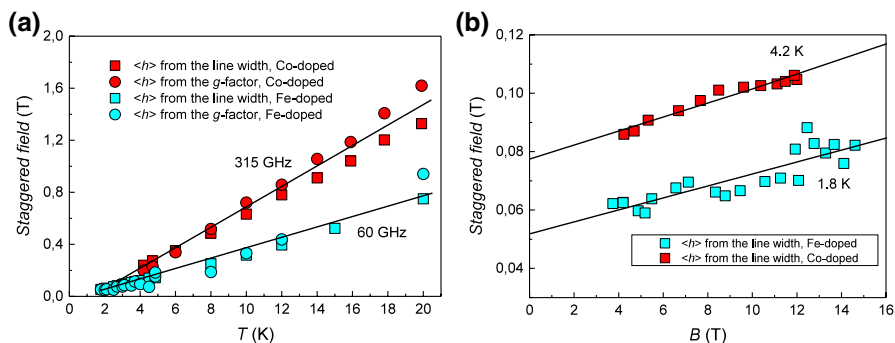


Fig. 12 Temperature dependence of the staggered field in $\text{CuGeO}_3:\text{Co}$ and $\text{CuGeO}_3:\text{Fe}$ from EPR measurements (a) and staggered field dependence of applied external magnetic field (b). Solid lines in the panel (a) are guides for the eyes; solid lines in the panel (b) are best fits with Eq. (20)

discrepancy can be easily explained in the following manner. Assuming that magnetic impurity moment scales as $\mu^* \sim g \cdot S \cdot \mu_B$ and neglecting difference in the g factors, we obtain that the ratio of magnetic impurity contributions for Co-doped and Fe-doped samples will be $\sim (3/2) \cdot 2\% / 2 \cdot 1\% = 1.5$, whereas the corresponding ratio $\langle h(0) \rangle$ will be 1.48 in fair agreement with the proposed estimate. Thus, although the μ^* magnitude for Co^{2+} ($S=3/2$) is less than for Fe^{2+} ($S=2$), the fact that impurity concentration in $\text{CuGeO}_3\text{:Co}$ is two times higher than in $\text{CuGeO}_3\text{:Fe}$ makes possible contribution from the impurity magnetic moment bigger in the Co-doped case.

Interestingly, experimental data on antiferromagnetic resonance in Ni- and Zn-doped CuGeO_3 reported in [42, 43] suggest a characteristic gap frequency about 20 GHz and spin-flop field about 1 T. Therefore, the magnetic fields characteristic to AF case, namely H_E and H_A [44], could be comparable with the $\langle h \rangle$ estimates presented in Fig. 12. In our opinion, this favors the idea about competition between interchain antiferromagnetic interactions and staggered Zeeman energy [36–38], which is characteristic of the aforementioned induction mechanism of the staggered field formation.

3.4 Staggered Field and Integrated Intensity

Everybody knows what is integrated intensity. To within a numerical coefficient, this quantity represents the spin part of the magnetic susceptibility [45]. And this really works, as long as experiment in CuGeO_3 demonstrates perfect coincidence of the static magnetic susceptibility with integrated intensity $\chi(T) \sim I(T)$ in a wide temperature range (Fig. 5). However, we will show that this fact is absolutely non-trivial, especially in the view of OA theory.

In statistical physics, the magnetic susceptibility is nothing but derivative by the field of the logarithm of a statistical sum multiplied by T/B ratio [46]. It must be stressed that the field-dependent energy levels used in the computation must be absolutely sharp and no tails in the density of states are allowed, as long as the opposite leads to the improper ground state [47].

In a single spin $S=1/2$ system described by the Hamiltonian

$$\hat{H}_Z = -g\mu_B \cdot B \cdot S^z, \quad (21)$$

the integrated intensity is given by [28]

$$I(\omega, B) = \frac{B_\omega^2 \omega}{2} \chi''(q=0, \omega, B), \quad (22)$$

where $\chi''(\omega)$ is the imaginary part of dynamic susceptibility $\chi(\omega) = \chi'(\omega) - i\chi''(\omega)$ and B_ω is the oscillating magnetic field. For the Hamiltonian (21), $\chi'' \sim \delta(\omega - \gamma_0 \cdot B)$ and EPR line is located at frequency $\gamma_0 B$ being sharp with zero width (here γ_0 denotes hydromagnetic ratio). In practice, EPR line somehow broadens, and δ -function may be replaced by Lorentzian or Gaussian without strict justification as it is done, for example, in [45]. However, we saw that the direct introduction of any relaxation parameter in quantum mechanical computation must be very accurate

due to the problem of the sharp levels and correct ground state mentioned before. Thus, the widely kept in mind qualitative picture when broad EPR line with finite width is due to transitions between broadened Zeeman levels may not be correct.

The situation is saved, when EPR is considered on the basis of semi-classical model implementing Landau–Lifshits equation for magnetization $M(B, T)$ motion [48]. In this case, the relaxation parameter α is introduced in a natural way and

$$\chi' = \chi_0 f'(\omega, B, \alpha), \quad \chi'' = \chi_0 f''(\omega, B, \alpha), \quad (23)$$

where $f'(\omega, B, \alpha)$, $f''(\omega, B, \alpha)$ are Lorentzian functions and $\chi_0 = M(B, T)/B$. The integration of the semi-classical line gives

$$I(T) \sim \int I(\omega, B) d\omega \sim \int I(\omega, B) dB \sim \chi_0. \quad (24)$$

In Eq. (24), the susceptibility χ_0 is taken at the resonant field B_{res} , thus justifying integrated intensity proportionality to static susceptibility. In that sense, $\chi(T) \sim I(T)$ is a semi-classical result rather than a quantum mechanical one.

In the OA theory, the Hamiltonian of the $S = 1/2$ interacting chain system in magnetic field has the form:

$$\hat{H} = \hat{H}_0 + \hat{H}_{\text{sf}} + \hat{H}_{\text{ea}} + \hat{H}_Z, \quad (25)$$

where

$$\hat{H}_0 = J \cdot \sum_{j,k} \vec{S}_j \cdot \vec{S}_k \quad (25a)$$

$$\hat{H}_Z = -B \cdot \sum_j S_j^z \quad (25b)$$

$$\hat{H}_{\text{sf}} = h \cdot \sum_j (-1)^j \cdot S_j^x \quad (25c)$$

$$\hat{H}_{\text{ea}} = \delta \cdot \sum_j S_j^x \cdot S_{j+1}^x. \quad (25d)$$

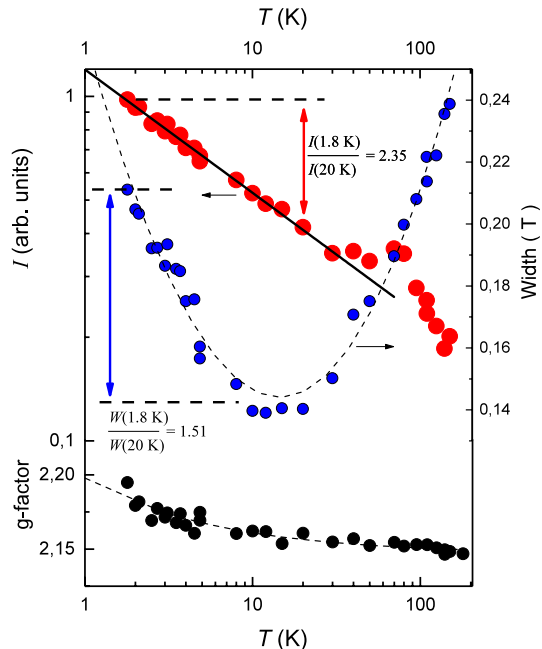
Apart from the exchange term describing AF interaction of spins in the chain (25a) and Zeeman term (25b), there are small anisotropic terms already discussed above, namely staggered field (25c) and exchange anisotropy (25d). The matter of fact is that in the absence of anisotropic term the problem with $\hat{H} = \hat{H}_0 + \hat{H}_Z$ still gives the EPR line in the form of δ function as in single ion case [27, 28]. This means that EPR line shape in a chain with strong interactions between magnetic ions will be given by δ function as in the non-interacting system. Strictly speaking, this circumstance excludes the applicability of exchange narrowing model for the description of the EPR line width in $S = 1/2$ AF quantum spin chain as it was often done in the past [42].

In OA theory, the finite line width appears as a result of the presence of the anisotropic terms (25c) and (25d) breaking the symmetry of the problem [27, 28]. In this approach, the EPR line shape is represented as an envelope of the infinite set of δ functions at EPR frequencies corresponding to the anisotropic terms in Hamiltonian. In this situation, there is no surprise that the parameters describing EPR line shape are correlated, which was established for the line width and g factor [29].

However, in the initial works [27, 28], the problem of integrated intensity was omitted. For that reason, we will turn to experimental data for $\text{CuGeO}_3\text{:Fe}$. Let us consider temperature diapason $T < 20$ K below line width minimum (Fig. 13). In this range, the contribution from staggered field dominates as it follows from the above analysis (Sects. 3.1, 3.2). At the same time, it is visible that in the interval $1.8 < T < 20$ K, the integrated intensity increases by 2.35 times, whereas the line width broadens by 1.51 times (Fig. 13). Thus, the change amplitude of the EPR absorption maximum (~ 1.56 times) is insufficient to get experimentally observed integrated intensity and in the considered diapason $I(T)$ are resulting from almost equal contributions from the amplitude and the width of the magnetic resonance. Consequently, at low temperatures in the studied system, the integrated intensity to a large extent is due to the presence of the staggered field and the link between staggered field and $I(T)$ promised at the end of section two is apparent.

At the same time, the condition $\chi(T) \sim I(T)$ holds (Fig. 5) and, therefore it is possible to conclude that staggered field term should contribute to static susceptibility and magnetization. However, staggered magnetic moment is aligned perpendicular to magnetization (Fig. 11) and, moreover, the sum of the staggered magnetic moments in the infinite chain is zero. So, the strong contribution from the staggered

Fig. 13 Temperature variation of the integrated intensity, line width and g factor in $\text{CuGeO}_3\text{:Fe}$



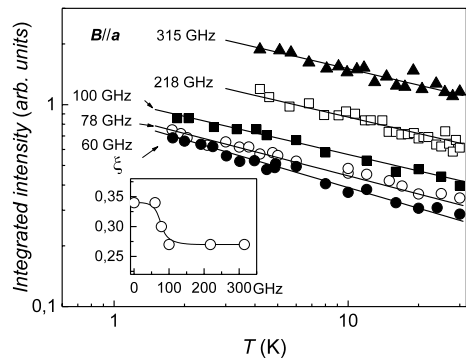
field to $I(T)$ and $\chi(T)$ is difficult to understand qualitatively at least for two reasons. First of all, “a contribution from line width” to susceptibility is not possible in the Zeeman levels broadening paradigm, as long as it contradicts the quantum statistical computation schema [46, 47]. Second, the geometry of the staggered component of magnetization excludes its magnetic response in direction of the applied magnetic field and thus could not affect susceptibility, which is opposite to the experimental situation. To our best knowledge, the considered paradox is not still resolved, and investigation of the relation of EPR integrated intensity and static magnetic susceptibility in the framework of the model (25) could be rewarding.

As a concluding remark, we wish to attract attention to the effect of measuring frequency influence on the exponent describing integrated intensity in the Griffiths phase $I(T) \sim 1/T^\xi$ [49]. For $\text{CuGeO}_3\text{:Fe}$ the slope of $\log I = f(\log T)$ curves decreases with frequency in the temperature interval $1.8 < T < 30$ K (Fig. 14). Thus, in the low-frequency range $\xi \sim 0.34$, whereas at high frequencies the exponent is about $\xi \sim 0.27$, i.e., this parameter decreases by $\sim 26\%$. The transition between low- and high-frequency asymptotics occurs in the vicinity 78–100 GHz (Fig. 14). At first glance, this behavior may be just trivial consequence of the magnetization saturation when magnetic field of the resonance is enhanced. However, in view of the above discussion of the staggered field contribution of the observed behavior may be attributed either to the change of the staggered field characteristics or to dynamical properties of spin clusters in the Griffiths phase.

4 New Magnetic Resonance and the Staggered Field

In OA theory, magnetic resonance in $S = 1/2$, 1D AF quantum spin chains should be treated as collective phenomenon rather than diffusive spin dynamics suggested by the exchange narrowing approach. In the case of electron paramagnetic resonance, the collective nature develops in the specific temperature dependences of the line width and g factor caused by the interplay of the staggered field and anisotropic exchange and in the damping of EPR at sufficiently low temperatures accompanied by rising of the breather mode [27, 28]. In the latter case, the changes in the resonant spectrum also affect the geometry of the experiment, namely EPR can be excited

Fig. 14 Frequency dependence of the integrated intensity (main panel) and change of the exponent describing temperature dependence of magnetic susceptibility in the Griffiths phase for $\text{CuGeO}_3\text{:Fe}$ (from Ref. [49])



only in Faraday geometry whereas breather mode may be observed for both Faraday and Voigt geometry [39].

Another possible field, where a collective motion of spins may be found, is the effect of polarization [28]. However, although both field theory approach [28] and direct numerical simulation [50] suggest that EPR line will depend on the orientation of the microwave field \mathbf{B}_ω , the expected influence on the line width and g factor is small. This result agrees well with the preceding calculations in the frame of the exchange narrowing theory and with the known experimental data [51–53]. These results can be easily qualitatively understood in the framework of the semi-classical approach, where the motion of the magnetization vector is circular in the plane perpendicular to the external field [48], and hence any alignment of \mathbf{B}_ω will cause a similar result for the excitation of the mode of the magnetic resonance.

This consistent picture was broken by the study of polarization characteristics of two resonances observed in $\text{CuGeO}_3\text{:Co}$ (Fig. 3). Strong polarization dependence for magnetic resonance A (Fig. 3) was discovered and investigated in detail in [54–56]. It was found that the discovered effect reflects the appearance of the unknown before collective mode in $S=1/2$ quasi 1D AF quantum spin chain. We wish to emphasize, that the resonance with anomalous polarization properties in $\text{CuGeO}_3\text{:Co}$ was not foreseen by any of the existing theories for low dimensional magnets, and have not received any theoretical explanation since first publication in 2006 [54]. We argue that the discovered effect reflects the appearance of the unknown before collective mode in $S=1/2$ quasi 1D AF quantum spin chain. Moreover, the observed dynamics of magnetization in this mode puts into question the universal character of Landau–Lifshits equation of motion, which is one of the cornerstones of modern magnetic resonance physics.

Cobalt magnetic impurity in CuGeO_3 ($S=3/2$) substitutes copper in chains [8, 10] and in contrast to the other dopants induces the onset of the specific resonant mode, which accompanies EPR on Cu^{2+} chains [8, 10]. The experimental spectrum of the resonant magnetoabsorption in $\text{CuGeO}_3\text{:Co}$ is formed by two broad lines, which can be completely resolved for frequencies $\omega/2\pi \geq 100$ GHz (Fig. 3). The frequencies of both modes are proportional to the resonant magnetic field in a wide range 60–360 GHz (Fig. 3). The analysis of the g factor values have shown that the resonant mode corresponding to higher magnetic fields (mode B) represents collective EPR on Cu^{2+} chains behaving in agreement with OA theory. Initially, the resonant mode corresponding to lower magnetic fields (mode A) was attributed to an EPR on Co^{2+} impurity clusters embedded into CuGeO_3 matrix [10].

However, it was first found in quasi-optical experiments that change of linear polarization of incident microwave radiation strongly affects the amplitude of the resonance A, whereas the amplitude of the resonance B remains conserved (Fig. 15). This effect was examined in detail by high-frequency cavity measurements, which for the considered problem have an advantage that allows avoiding depolarization of radiation in the light pipe. Three cases, when \mathbf{B} was aligned along \mathbf{a} , \mathbf{b} and \mathbf{c} crystallographic direction, were studied. In each case, the two orientations of oscillating microwave field along remaining axes were investigated, namely for $\mathbf{B} \parallel \mathbf{a}$ the polarizations $\mathbf{B}_\omega \parallel \mathbf{b}$ and $\mathbf{B}_\omega \parallel \mathbf{c}$, and so on. Thus, six experimental geometries were investigated (Fig. 16). In addition, for $\mathbf{B} \parallel \mathbf{a}$, the

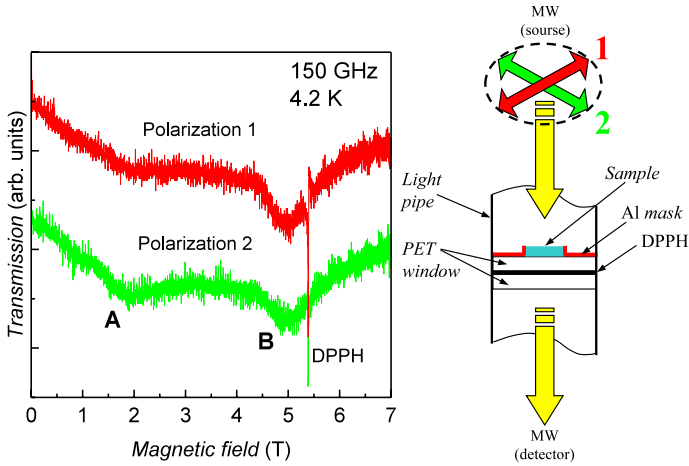


Fig. 15 Polarization dependence of the resonance A in $\text{CuGeO}_3\text{:Co}$ in quasi-optical experiment (the data are from Ref. [55])

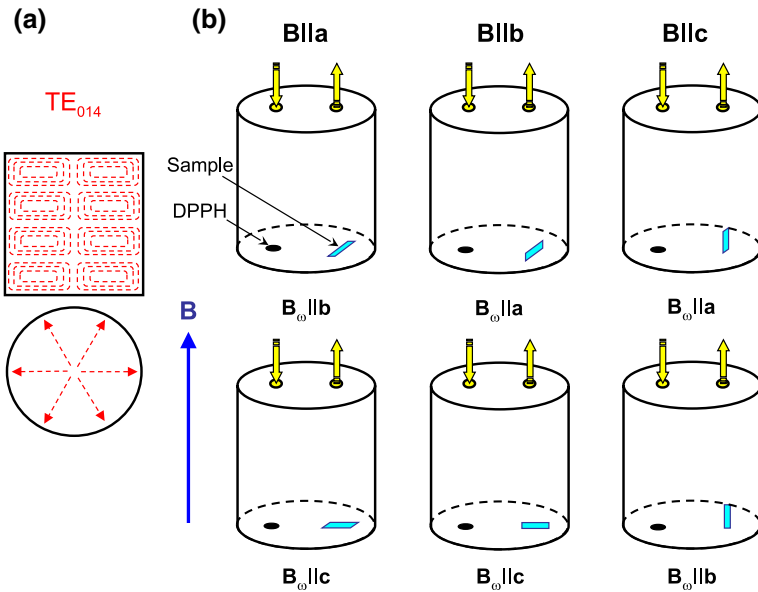


Fig. 16 Oscillating magnetic field for TE_{014} cavity mode (a) and six experimental geometries for investigation of polarization effect (b)

measurements with rotation of the sample inside the cavity were performed. To achieve a high frequency ~ 100 GHz, the cylindrical cavity was operating at TE_{014} mode. A small DPPH reference sample was simultaneously placed in the cavity [54–56].

It is worth to note that in all cases studied $\mathbf{B}_\omega \perp \mathbf{B}$ and no strong anisotropy effect in convenient EPR is expected in either OA theory or semi-classical description of the magnetic resonance. However, the data obtained in [54–56] contradict to this picture. It is visible from Fig. 17 that low-field mode A, which was supposed to be “impurity” resonance in the previous studies [8, 10], can be excited for one polarization only. At the same time, the EPR on Cu^{2+} chains (resonance B) does not show any strong polarization dependence. For mode A and $\mathbf{B} \parallel \mathbf{a}$, an “active” polarization will be $\mathbf{B}_\omega \parallel \mathbf{c}$ and “non-active” polarization corresponds to the case $\mathbf{B}_\omega \parallel \mathbf{b}$ (Fig. 17a). It is worth to note that in “non-active” polarization the magnetic resonance A is almost completely damped, and weak traces of this mode for $\mathbf{B}_\omega \parallel \mathbf{b}$, which are visible at low temperatures, are due to the finite sample size and related weak misalignment of \mathbf{B}_ω from \mathbf{b} -axis in cavity measurements. Another characteristic feature of the observed phenomenon is the peculiar temperature dependence. For “active” case mode A appears below 40 K and at $T \sim 12$ K becomes as strong as the resonance on Cu^{2+} chains. Further lowering of temperature makes the A resonance a dominating feature in the magnetoabsorption spectrum, having amplitude considerably exceeding that of mode B (Fig. 17b).

In order to confirm the selected character of just one direction the experiment with the sample rotation inside the cavity was carried out for $\mathbf{B} \parallel \mathbf{a}$ (Fig. 18). Observed angular dependence of the mode A amplitude is well described by cosine law [55], suggesting that only projection of \mathbf{B}_ω on the \mathbf{c} axis is responsible for the excitation of this resonance.

Similar to the case $\mathbf{B} \parallel \mathbf{a}$ behavior has been observed for $\mathbf{B} \parallel \mathbf{b}$ geometry (Fig. 19). In this case for mode A, an “active” polarization is $\mathbf{B}_\omega \parallel \mathbf{a}$, and “non-active” polarization is $\mathbf{B}_\omega \parallel \mathbf{c}$, whereas the resonance B is not much affected by the orientation of the microwave field. In agreement with the case $\mathbf{B} \parallel \mathbf{a}$, the mode A is the strongest in

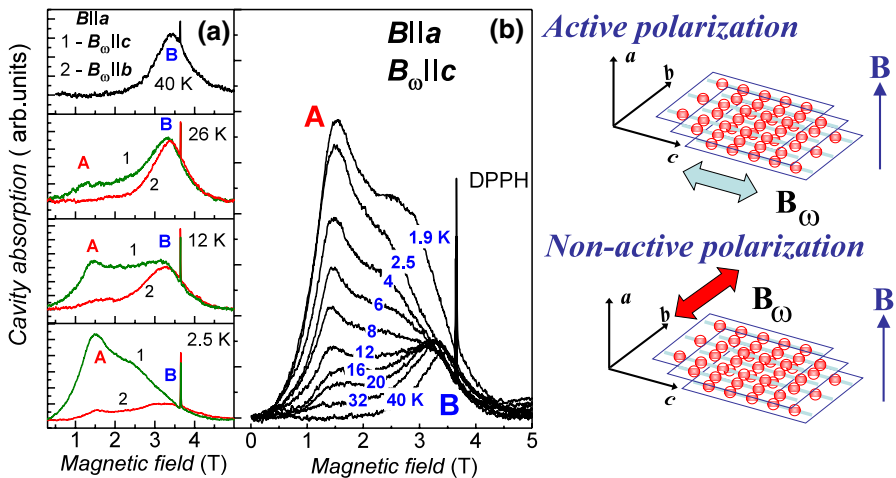


Fig. 17 Resonant magnetoabsorption spectra in geometry $\mathbf{B} \parallel \mathbf{a}$ at 100 GHz for active ($\mathbf{B}_\omega \parallel \mathbf{c}$) and non-active ($\mathbf{B}_\omega \parallel \mathbf{b}$) polarizations at various temperatures (panel a) and temperature dependence in the case of active polarization (panel b). From Ref. [54–56]

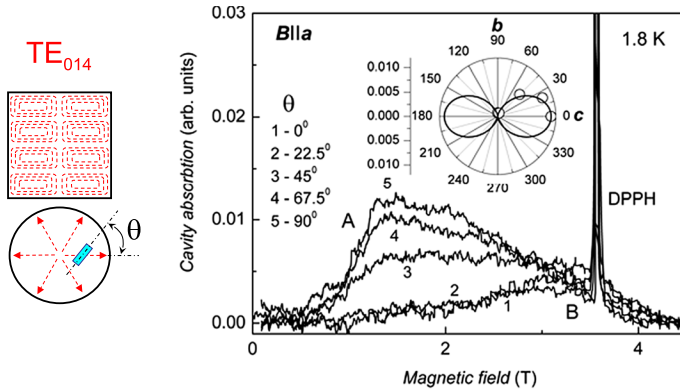


Fig. 18 Experiment with the sample rotation inside the cavity at 100 GHz for $B||a$. The angle θ is measured from the c -axis. Polar plot in the inset represents the comparison of the angular dependence of the resonance A magnitude (points) with the cosine law (solid line). From Ref. [55]

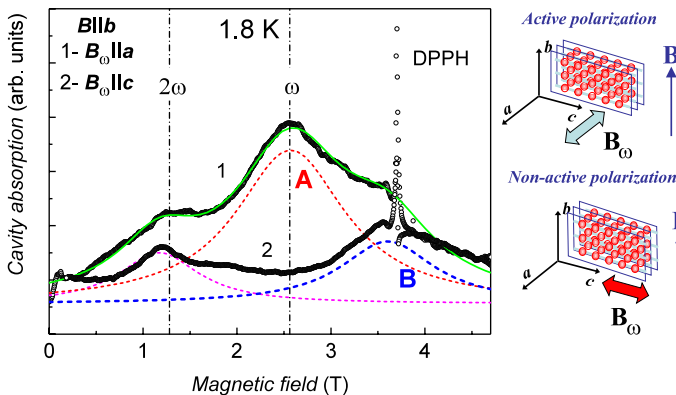


Fig. 19 Resonant magnetoabsorption spectra at 100 GHz in geometry $B||b$ for active ($B_{\omega}||a$, curve 1) and non-active ($B_{\omega}||c$, curve 2) polarizations [54, 55]. Dashed lines show deconvolution of the spectrum for active polarization into three components (resonances A, B, and the second harmonic of the resonance A). Solid line represents the sum of the spectral components. Details of the deconvolution procedure are provided in Ref. [55]

the spectrum; however, for $B||b$, the main resonance A is accompanied by its second harmonic (Fig. 19). Interestingly, although the mode A is completely damped in $B_{\omega}||c$ case, the second harmonic of this resonance retains the same amplitude for both “active” and “non-active” polarizations (Fig. 19). More details about the structure of the resonance line can be found in [55].

A dominating character of the resonance A at low temperatures is conserved in $B||c$ case (Fig. 20). However, the effect of polarization appears to be weaker, and for $B_{\omega}||b$, the amplitude of the resonance A is only two times less than for $B_{\omega}||a$. Nevertheless, the polarization dependence of this mode remains anomalously strong, especially as compared with the resonance on Cu^{2+} chains.

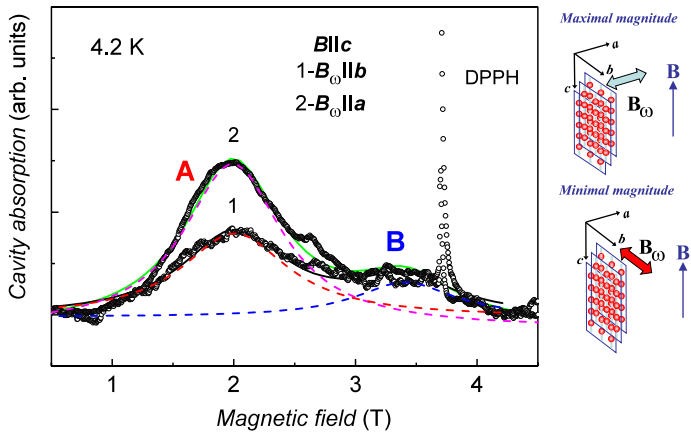


Fig. 20 Resonant magnetoabsorption spectra at 100 GHz in geometry $B||c$ for polarizations $B_{\omega}||b$ (curve 1) and $B_{\omega}||a$, (curve 2) [54, 55]. Dashed lines show deconvolution of the spectrum for $B_{\omega}||a$, into components corresponding to the resonances A and B. Solid line represents the sum of the spectral components for $B_{\omega}||b$ and $B_{\omega}||a$. Details of the deconvolution procedure are provided in Ref. [55]

Data in Figs. 17, 19, and 20 show that the resonance field for the mode A varies substantially, when the direction of the external magnetic field B is changed. The corresponding g factor values are $g \approx 4.9$ ($B||a$), $g \approx 2.9$ ($B||b$) and $g \approx 3.7$ ($B||c$). Thus, the g factor for this mode may differ 1.7 times, while for the EPR on Cu^{2+} chains (resonance B) the g factors for various crystallographic directions lie in the range $\sim(2.06-2.26)$ and hence are changed only by 10% [54].

The experimental data obtained in the present work with no doubts demonstrate that the resonant mode A in $CuGeO_3:Co$ is an anomalous one. First of all, this mode shows extremely strong dependence on the orientation of the oscillating microwave field B_{ω} in Faraday geometry. At the same time, no comparable effect for EPR on Cu^{2+} chains is observed in good agreement with any theoretical expectations.

Second, the vanishing of the resonance A for certain polarizations means that the character of magnetic oscillations in this mode is completely different from the precession of the magnetization vector around the magnetic field direction described by Landau–Lifshits equation. Indeed in case of precession, the magnetization vector end moves around a circle, whose plane is perpendicular to the magnetic field, and hence *any* linear polarization in Faraday geometry will excite EPR-like mode or any mode based on correlated precession of various magnetization components.

Thirdly, modes A and B coexist in a wide temperature range $1.8 < T < 40$ K that excludes possible explanation based on breather scenario for collective mode [27, 28, 39], where EPR (mode B) should vanish after the onset of the breather excitation like in the case of Cu-benzoate. The onset of mode A at relatively high temperatures $T \sim 40$ K (Fig. 17) simultaneously eliminates applicability of the standard scenario of doping [6], where the coexistence of EPR and antiferromagnetic resonance (AFMR) in doped $CuGeO_3$ may be expected only at temperatures below $0.3 T_{SP} \sim 4$ K (in experiments AFMR coexisting with EPR in $CuGeO_3$ have been observed at $T < 2$ K [43]).

The above consideration does not allow explaining mode A in terms of a single spin EPR problem. At the same time, the properties of this magnetic resonance are not possible to describe assuming either collective EPR or AFMR in quantum spin chains system, as well by other known to date collective modes like breather excitations. Thus, the doping with Co of Cu^{2+} quantum spin chains in CuGeO_3 leads to the formation of *unidentified novel magnetic resonance*. Nevertheless, it is possible to deduce that the observed excitation of magnetic subsystem of $\text{CuGeO}_3:\text{Co}$ has a collective nature. The first argument favoring this supposition is the magnitude of this magnetic resonance. Taking into account that in the samples studied only 2% of copper ions are substituted by cobalt impurity, and no spin-Peierls transition affecting mode B happens, it is difficult to expect that any individual impurity mode will considerably exceed the magnitude of the magnetic resonance on Cu^{2+} chains (Figs. 17, 18, 19, 20). Therefore, in our opinion, mode A is likely a specific collective excitation of quasi-1D Cu^{2+} chain, which properties are modified by doping.

The unusual polarization dependence of mode A may be considered as another argument. Apparently, the observed behavior is forbidden for a single spin or $S = 1/2$ AF spin chain with the Hamiltonian with small anisotropic perturbations [27, 28]. However, in the presence of anisotropic terms, the spin chain Hamiltonian will no longer commute with the magnitude of the total spin and its z component, and hence, in principle, the magnetic oscillation modes different from the standard spin precession may become possible. It is worth to note that experimental data in Figs. 17, 18, 19 and 20 suggest a selected character of the \mathbf{b} axis. Indeed, for $\mathbf{B}_\omega \parallel \mathbf{b}$ the resonance A is completely damped ($\mathbf{B} \parallel \mathbf{a}$) or its magnitude is reduced ($\mathbf{B} \parallel \mathbf{c}$) and in case $\mathbf{B} \parallel \mathbf{b}$ second harmonic of the anomalous mode, which is missing in other geometries, develops. As we have shown, the \mathbf{b} -axis is an “easy axis” for a staggered field (Sect. 3). Therefore, the observed mode A is likely somehow related to the staggered field, which may be responsible for anomalous polarization characteristics. However, from the theoretical point of view, the staggered field is known to be an anisotropic term in Hamiltonian, which is crucial for the EPR problem in the studied case (Sect. 3) and it is not clear what kind of mechanism should be involved to link staggered field and new magnetic excitation discovered in [54–56]. The absence of the explanation of the new type of magnetic resonance to date from one hand demonstrates the difficulty in accounting of this phenomenon as well as the incomplete character of the EPR theory in quantum spin chains.

From the data presented in Figs. 17, 18, 19 and 20, it is possible to deduce the character of magnetic oscillations for resonances A and B in $\text{CuGeO}_3:\text{Co}$ assuming semi-classical approximation [54–56], where the magnetization in given magnetic field \mathbf{B} has a form $\mathbf{M} = \mathbf{M}_0 + \mathbf{m}$. Here \mathbf{M}_0 denotes an equilibrium value and \mathbf{m} stands for the oscillating part [48]. As long as magnetic resonance probes normal modes of magnetization oscillations described by vector \mathbf{m} , for excitation of some mode vectors, \mathbf{B}_ω should have non-zero projection on any \mathbf{m} component [48], i.e., condition $(\mathbf{B}_\omega, \mathbf{m}) \neq 0$ for the scalar product should be fulfilled. For geometry $\mathbf{B} \parallel \mathbf{a}$ and normal mode, where precession of magnetization around field direction takes place, $\mathbf{m} = (0, m_b, m_c)$ and both projections of \mathbf{m} on \mathbf{b} - and \mathbf{c} -axes are non-zero. Therefore, any alignment of vector \mathbf{B}_ω in \mathbf{b} - \mathbf{c} plane will excite precession. The weak dependence of the resonance amplitude on \mathbf{B}_ω alignment corresponds to condition $m_b \approx m_c$. Thus,

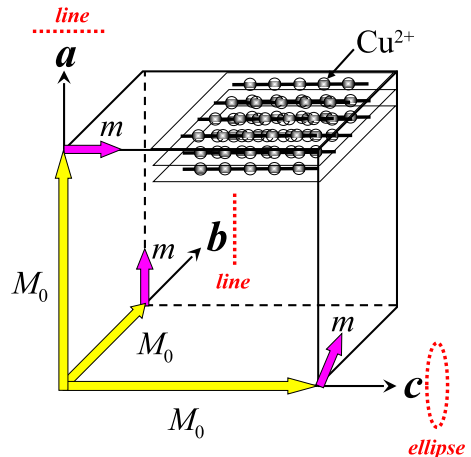
for the mode B and $\mathbf{B}\parallel\mathbf{a}$ the trajectory of the vector end is a circle lying in the $\mathbf{b}-\mathbf{c}$ plane (similar consideration is apparently applicable to mode B in geometries $\mathbf{B}\parallel\mathbf{b}$ and $\mathbf{B}\parallel\mathbf{c}$).

The same analysis can be applied for resonance A. Data in Figs. 17 and 18 suggest that in geometry $\mathbf{B}\parallel\mathbf{a}$, the oscillating contribution to magnetization should acquire the form $\mathbf{m}=(0, 0, m_c)$ leading to “active” polarization $\mathbf{B}_\omega\parallel\mathbf{c}$ and “non-active” polarization $\mathbf{B}_\omega\parallel\mathbf{b}$ (Figs. 17, 18). Therefore, in this case, the end of vector \mathbf{M} should move along a line parallel to \mathbf{c} -axis. Analogously $\mathbf{m}=(m_a, 0, 0)$ for $\mathbf{B}\parallel\mathbf{b}$ and linear oscillation will happen along \mathbf{a} -axis. For $\mathbf{B}\parallel\mathbf{a}$, mode A can be excited in both polarizations and hence $\mathbf{m}=(m_a, m_b, 0)$. However, the decrease of the resonance magnitude for $\mathbf{B}\parallel\mathbf{c}$ suggests condition $m_a \approx 2m_b$ (Fig. 20). As a result, the trajectory of the vector \mathbf{M} will be an ellipse in the $\mathbf{a}-\mathbf{b}$ plane elongated in \mathbf{a} -direction. The summary of the above consideration for mode A is given in Fig. 21. We wish to add that in some cases, trajectories of vector \mathbf{M} end may be even more complicated due to the observation of second harmonic (Fig. 19) as well of possibility of combination frequencies (see [55]). Thus, Fig. 21 represents a simplest possible variant for magnetization dynamics in mode A.

The experimental data in Figs. 10, 11, 12, 13, 14, 15, 16 and 17 suggest that the resonant fields and hence the g values of the mode A are rather anisotropic. The anisotropy of the g factor may correspond to the Co^{2+} magnetic ion in the octahedral ligand field. In turn, in the presence of the anisotropic g factor, the precession motion of the magnetization vector will be deformed from circular to ellipsoid. This explanation may be applied to the case $\mathbf{B}\parallel\mathbf{c}$, where the elliptic movement of the magnetization vector is indeed observed (Figs. 20, 21). However, the above idea is hardly applicable to linearly polarized magnetic oscillations found for $\mathbf{B}\parallel\mathbf{a}$ and $\mathbf{B}\parallel\mathbf{b}$.

To our best knowledge, the modes with linear oscillation trajectories have been neither reported for any magnetic resonance nor foreseen by theoretical studies. Moreover, the current understanding of the whole field of magnetic resonance (including electron paramagnetic, antiferromagnetic and ferromagnetic resonance) essentially exploit semi-classical magnetization precession in an external field, and

Fig. 21 Summary of the modes of magnetic oscillations of the resonance A corresponding to the different alignment of the external magnetic field with respect to crystal axes. Dotted lines mark the trajectory at which the magnetization vector is expected to move (from Ref. [54–56])



hence hardly leaves space to observe new polarization effect. Therefore, an adequate theory relevant to the studied case, including different polarization characteristics of magnetic resonance harmonics, appears on the agenda.

5 Conclusions

Our excursion to the forgotten field of CuGeO_3 demonstrates that studying this material put forward many interesting and still actual problems, which are not resolved in physics of quantum spin chain systems up to now. We see that uncritical direct use of either semi-classical models or exchange narrowing theory may cause misleading results for collective EPR on correlated ensemble of spins in the chain. Fortunately, for $S = 1/2$ AF 1D chain there is the lodestar, namely the theory developed by Oshikawa and Affleck. The application of their approach shows that most interesting physical phenomena are localized around staggered field, which appears as a driving force in the onset of anomalous growth of the line width and g factor at low temperatures. At the same time, the possible role of the staggered field is not confined to this problem and its influence may be seen in a variety of phenomena from the peculiar temperature dependence of the magnetic susceptibility in disorder-driven quantum critical Griffiths phase to a new type of magnetic oscillations.

Although the unique among EPR theories universal relation between the line width and g factor, which follows from the OA theory, provides a unique tool for studying of the staggered field, the experiment seems to run ahead far from theoretical state of the art. In that sense, it is necessary to mention (i) the origin of the staggered field in various experimental systems and its dependence on temperature and external magnetic field; (ii) the non-trivial problem of integrated intensity; as well as (iii) the nature and limits of applicability of the universal relation.

Special attention deserves the Griffiths phase, which may be induced in CuGeO_3 by doping with magnetic impurities. This phase seems to be constructed of nanoclusters, but this view on this quantum critical phase is far from the main way of theories for quantum criticality. Interestingly, in [57], it was found that the reduction of the crystallite's size to nanometer scale (300×30 nm) leads to full suppression of spin-Peierls transition in pure (undoped) CuGeO_3 . Simultaneously, the temperature dependence of EPR integrated intensity in nano- CuGeO_3 acquires almost the same as for 1% Fe-doped CuGeO_3 and thus germanium cuprate in the nano-world exhibit behavior typical of QC Griffiths phase. This finding links old-fashioned CuGeO_3 with the modern nanomagnetic problematic.

Last but not least is the new type of magnetic oscillations, as long as it seems having explanation neither in OA theory nor within the framework of the semi-classical magnetization motion. This "enfant terrible" of CuGeO_3 physics poses the most difficult case and touchstone for a theory; as long as experimentally observed modes of magnetic oscillations are likely in contradiction to Landau–Lifshits equation of motion.

In our opinion, the return to the current scientific agenda of germanium cuprate has every chance to confirm the adage that the new is the well-forgotten old, especially in the field of quantum spin chains.

Acknowledgements The authors are grateful to Dr. A.N. Samarin for his help with manuscript preparation. This work was supported by Programme of Russian Academy of Sciences "Photon technologies in probing of inhomogeneous media and biological objects".

References

1. M. Hase, I. Terasaki, K. Uchinokura, M. Tokunaga, N. Miura, H. Obara, Phys. Rev. B **48**, 9616 (1993)
2. K. Uchinokura, M. Hase, Y. Sasago, Phys. B **211**, 175 (1995)
3. L.P. Regnault, M. Ain, B. Hennion, G. Dhalle, A. Revkolevski, Phys. Rev. B **53**, 5579 (1996)
4. M. Hase, Y. Sasago, I. Terasaki, K. Uchinokura, G. Kido, T. Hamamoto, J. Phys. Soc. Jpn. **65**, 273 (1996)
5. H. Nojiri, T. Hamamoto, Z.J. Wang, S. Mitsudo, M. Motokawa, S. Kimura, H. Ohta, A. Ogiwara, O. Fujita, J. Akimitsu, J. Phys. Condens. Matter **9**, 1331 (1997)
6. M. Mostovoy, D. Khomskii, J. Knoester, Phys. Rev. B **58**, 8190 (1998)
7. S.V. Demishev, R.V. Bunting, L.I. Leonyuk, E.D. Obraztsova, A.A. Pronin, N.E. Sluchanko, N.A. Samarin, S.V. Terekhov, JETP Lett. **73**, 31 (2001)
8. S.V. Demishev, Y. Inagaki, M.M. Markina, H. Ohta, S. Okubo, Y. Oshima, A.A. Pronin, N.E. Sluchanko, N.A. Samarin, V.V. Glushkov, Phys. B **329**, 715 (2003)
9. S.V. Demishev, A.V. Semeno, A.A. Pronin, N.E. Sluchanko, N.A. Samarin, H. Ohta, S. Okubo, M. Kimata, K. Koyama, M. Motokawa, A.V. Kuznetsov, J. Supercond. Novel Magn. **20**, 105 (2007)
10. S.V. Demishev, A.V. Semeno, N.E. Sluchanko, N.A. Samarin, A.A. Pronin, Y. Inagaki, S. Okubo, H. Ohta, Y. Oshima, L.I. Leonyuk, Phys. Solid State **46**, 2238 (2004)
11. S.V. Demishev, A.V. Semeno, N.E. Sluchanko, N.A. Samarin, I.E. Tarasenko, H. Ohta, S. Okubo, Appl. Magn. Reson. **35**, 327 (2008)
12. R.B. Griffiths, Phys. Rev. Lett. **23**, 17 (1969)
13. A.J. Bray, Phys. Rev. Lett. **59**, 586 (1987)
14. D.S. Fisher, Phys. Rev. Lett. **69**, 534 (1992)
15. D.S. Fisher, Phys. Rev. B **50**, 3799 (1994)
16. D.S. Fisher, Phys. Rev. B **51**, 6411 (1995)
17. S.V. Demishev, Phys. Solid State **51**, 547 (2009)
18. S.V. Demishev, Phys. Status Solidi B **247**, 676 (2010)
19. S.V. Demishev, A.L. Chernobrovkin, V.V. Glushkov, A.V. Grigorieva, E.A. Goodilin, H. Ohta, S. Okubo, M. Fujisawa, T. Sakurai, N.E. Sluchanko, N.A. Samarin, A.V. Semeno, Phys. Rev. B **84**, 094426 (2011)
20. S.V. Vonsovskii, *Magnetism* (Wiley, New York, 1979)
21. H. Reiger, A.P. Young, Phys. Rev. B **54**, 3328 (1996)
22. A. Abragam, B. Bleaney, *Electron Paramagnetic Resonance of Transition Ions* (Clarendon Press, Oxford, 1970)
23. R. Kubo, K. Tomita, J. Phys. Soc. Jpn. **9**, 888 (1954)
24. H. Mori, K. Kawasaki, Prog. Theor. Phys. **27**, 529 (1962)
25. H. Mori, K. Kawasaki, Prog. Theor. Phys. **28**, 971 (1962)
26. K. Okuda, H. Hata, M. Date, J. Phys. Soc. Jpn. **33**, 1574 (1972)
27. M. Oshikawa, I. Affleck, Phys. Rev. Lett. **82**, 5136 (1999)
28. M. Oshikawa, I. Affleck, Phys. Rev. B **65**, 134410 (2002)
29. S.V. Demishev, Y. Inagaki, H. Ohta, S. Okubo, Y. Oshima, A.A. Pronin, N.A. Samarin, A.V. Semeno, N.E. Sluchanko, Europhys. Lett. **63**, 446 (2003)
30. J. Lüdecke, A. Jobst, S. van Smaalen, E. Morre, C. Geibel, H.-G. Krane, Phys. Rev. Lett. **82**, 3633 (1999)
31. T. Asano, H. Nojiri, Y. Inagaki, J.P. Boucher, T. Sakon, Y. Ajiro, M. Motokawa, Phys. Rev. Lett. **84**, 5880 (2000)
32. F.H.L. Essler, A.M. Tselik, Phys. Rev. B **57**, 10592 (1998)
33. F.H.L. Essler, Phys. Rev. B **59**, 14376 (1999)
34. K. Nagata, Y. Tazuke, J. Phys. Soc. Jpn. **32**, 337 (1972)
35. K. Nagata, Y. Tazuke, J. Phys. Soc. Jpn. **38**, 1003 (1975)

36. S. Demishev, A. Semeno, A. Pronin, N. Sluchanko, N. Samarin, H. Ohta, S. Okubo, M. Kimata, K. Koyama, M. Motokawa, Prog. Theor. Phys. Suppl. **159**, 387 (2005)
37. S.V. Demishev, A.V. Semeno, A.A. Pronin, N.E. Sluchanko, N.A. Samarin, H. Ohta, S. Okubo, M. Kimata, K. Koyama, M. Motokawa, A.V. Kuznetsov, J. Magn. Magn. Mater. **300**, e346 (2006)
38. M. Sato, M. Oshikawa, Phys. Rev. B **69**, 054406 (2004)
39. Y. Ajiro, J. Phys. Soc. Jpn. **72**(Suppl. B), 12 (2003)
40. H. Ohta, K. Kawakami, Y. Inagaki, S. Okubo, T. Kunimoto, Z. Hiroi, Prog. Theor. Phys. Suppl. **145**, 95 (2002)
41. H. Ohta, S. Okubo, K. Kawakami, D. Fukuoka, Y. Inagaki, T. Kunimoto, Z. Hiroi, J. Phys. Soc. Jpn. **72**(Suppl B), 26 (2003)
42. V.N. Glazkov, A.I. Smirnov, O.A. Petrenko, D. McK Paul, A.G. Vetkin, R.M. Eremina, J. Phys. Condens. Matter **10**, 7879 (1998)
43. A.I. Smirnov, V.N. Glazkov, A.N. Vasilev, L.I. Leonyuk, S.M. Coad, D. McK Paul, G. Dhalenne, A. Revcolevschi, JETP Lett **64**, 305 (1996)
44. F. Keffer, C. Kittel, Phys. Rev. **85**, 329 (1952)
45. S.A. Al'tshuler, B.M. Kozyrev, *Electron Paramagnetic Resonance* (Academic Press, New York, 1964)
46. I.A. Kvasnikov, *Thermodynamics and Statistical Physics. The Theory of Equilibrium Systems. Statistical Physics*, vol. 2 (Editorial URSS, Moscow, 2002) (**in Russian**)
47. R. Kubo, H. Ichimura, T. Usui, N. Hashitsume, *Statistical Mechanics* (North Holland, Amsterdam, 1990)
48. A.G. Gurevich, G.A. Melkov, *Magnetization Oscillations and Waves* (CRC Press, Boca Raton, 1996)
49. S.V. Demishev, A.V. Semeno, N.E. Sluchanko, N.A. Samarin, A.A. Pronin, V.V. Glushkov, H. Ohta, S. Okubo, M. Kimata, K. Koyama, M. Motokawa, A.V. Kuznetsov, Phys. B **359**, 1315 (2005)
50. S. Miyashita, T. Yoshino, A. Ogasahara, J. Phys. Soc. Jpn. **68**, 655 (1999)
51. Y. Natsume, F. Sasagawa, M. Toyoda, I. Yamada, J. Phys. Soc. Jpn. **48**, 50 (1980)
52. I. Yamada, Y. Natsume, J. Phys. Soc. Jpn. **48**, 58 (1980)
53. Y. Natsume, F. Noda, F. Sasagawa, H. Kanazawa, J. Phys. Soc. Jpn. **52**, 1427 (1983)
54. S.V. Demishev, A.V. Semeno, H. Ohta, S. Okubo, I.E. Tarasenko, T.V. Ishchenko, N.E. Sluchanko, JETP Lett. **84**, 249 (2006)
55. S.V. Demishev, A.V. Semeno, H. Ohta, S. Okubo, I.E. Tarasenko, T.V. Ishchenko, N.A. Samarin, N.E. Sluchanko, Phys. Solid State **49**, 1295 (2007)
56. A.V. Semeno, H. Ohta, S. Okubo, N.E. Sluchanko, I.E. Tarasenko, A.V. Kuznetsov, T.V. Ishchenko, S.V. Demishev, Appl. Magn. Reson. **33**, 3 (2008)
57. A.V. Semeno, M.I. Gilmanov, A.V. Kuznetsov, N.N. Melnik, A.V. Grigorjeva, A.V. Barulin, E.A. Gudilin, S.V. Demishev, Appl. Magn. Reson. **47**, 881–893 (2016)

Publisher's Note Springer Nature remains neutral with regard to jurisdictional claims in published maps and institutional affiliations.